RSC Advances

ROYAL SOCIETY OF CHEMISTRY

www.rsc.org/advances

Table of contents entry

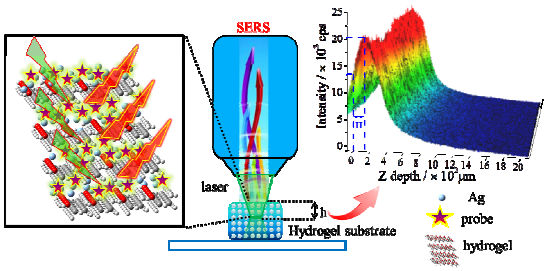

A facile strategy was developed to fabricate a three dimensional (3D) hydrogel decorated with Ag nanoparticles as SERS substrate. A macro effective depth in this 3D network was confirmed by slice observation and depth scanning. The free-standing flexible substrate produced satisfactory results with excellent sensitivity and reproducibility in analysis of trace environmental molecules.

RSC Advances

RSCPublishing

ARTICLE

Three-Dimensional Plasmonic Hydrogel Architecture: Facile Synthesis and Its Macro Scale Effective Space

Cite this: DOI: 10.1039/xoxxoooooox

Received ooth January 2012,
Accepted ooth January 2012

DOI: 10.1039/xoxxoooooox

www.rsc.org/

Lei Ouyang,[a,b] Lihua Zhu,*[a] Jizhou Jiang,[a] Wei Xie[c] and Heqing Tang*[b]

A three dimensional (3D) hydrogel SERS substrate decorated with Ag nanoparticles (NPs) was fabricated by in situ reducing Ag^+ ions in polyvinyl alcohol (PVA) network. This offered tuneable, easily-operational and extremely homogeneous SERS 3D substrates composed of uniformly distributed Ag NPs. Due to its good light penetration, a macro effective space with a depth of more than one hundred micrometres in this translucent 3D network was confirmed by slice observation and depth scanning techniques. Such macro effective space may come from harvesting plasmonic effects between active Ag NPs couplings in all of the x, y, and z directions, resulting in great average field within the whole substrate region. Due to its giant effective depth, the 3D hydrogel is more sensitive and more tolerable toward out-of-focus laser position at the sample for trace detection. The free-standing and flexible structure is also employed in environmental analysis by using a portable Raman instrument, showing its promising potential for real applications.

Introduction

Surface–enhanced Raman spectroscopy (SERS) shows diverse applications in many fields such as chemical identification,[1] food safety,[2] environmental protection,[3] reaction mechanism study,[4] bio-imaging,[5] and bio-analysis.[6] Since SERS comes from the excitation of localized metal surface plasmon resonances of a substrate,[7] the enhancing effect highly depends on the property of the substrate.[8] The recent progress in SERS substrates is attributed to improvements in nanofabrication techniques.[9] However, great challenges still remain in new strategies of developing SERS substrates which exhibit highly sensitive and reproducible responses and are easily operated in practical applications.[10]

The substrates involved in earlier studies were nanoparticles (NPs).[11] Later, nanorods and nanowires were used as one dimensional (1D) substrates.[12] Two dimensional (2D) substrates were nano blocks arranged orderly on a support,[13] for example Ag NPs immobilized magnetic Fe_3O_4 NPs or SiO_2 microspheres.[14] Because optical scattering and light collection occur in a three dimensional (3D) volume, assembly and templating techniques can create structures that confine electric field within the entire region in a 3D space, which is defined as a 3D substrate.[15] Within the 3D volume the greatest average field enhancement rather than the greatest absolute field enhancement would maximize the generation and collection of SERS signal, thus 3D substrates provide a new strategy for more sensitive SERS performance. [16]

A way to prepare a 3D substrate was to decorate NPs on a 1D or 2D template.[17] Examples include a 3D substrate with Au NPs on the walls of vertically aligned CNTs,[18] and a 3D biomimetic substrate on the bioscaffold arrays of cicada wings.[19] This type of 3D substrates requires additional supports to support the concerned 3D space. Another way involves a bottom-up method: a silver nanowire 3D structure was fabricated by layer-by-layer assembling method,[20] and a 3D nanostructure of Au nanostars on silicon pillars was obtained by sputtering.[21] Although these 3D structures produced outstanding sensitivity for the SERS detection of the analytes (with enhancement coefficient up to 10^7), they often required complex fabrication procedures such as ion etching and sputter coating. To evaluate the real 3D space property of SERS substrates, we proposed a concept of "effective depth", which represents the depth in 3D volume that contributes to the SERS signal collected (the difference between "effective depth" and the conventional "active depth" can be found in ESI). For above mentioned substrates, their effective depths were limited to hundreds nanometers (for example: 300 nm[20] and 150 nm[21]) because the support material had poor light transparency or the metal NPs were decorated in only the outmost surface layer. Therefore, these 3D substrates may be referred to nano-scale 3D SERS substrates.

It is known the penetration depth of lasers may expand to several millimetres in proper materials.[22] These nano-scale 3D SERS substrates with limited effective depth would hide the superiority of the 3D structures. If the effective depth is further increased, more plasmonic sites can enhance the excitation light trapping in the 3D structure, and more target molecules and more efficient light-matter interaction in the effective volume will contribute to greater enhancement. Therefore, it is very important to develop new 3D structures with greater effective depths.

Noble metal NPs encapsulated hydrogels may perform as a new type of 3D substrates. Bao et al. prepared a SERS substrate by using alginate gel adsorbed with Au NPs.[23] Manikas et al. reported a SERS

substrate in which self-assembled Au NPs were physisorbed on poly(N-isopropylacrylamide) thermo-responsive hydrogels.[24] These two substrates may be taken as 2D ones because the effective Au NPs were only adsorbed on the surface but not in the bulk of the gel. Shin et al. reported Au NP-encapsulated poly(acrylic acid) gel as a SERS substrate.[25] Park et al reported bacterial cellulose hydrogels containing Au NPs for SERS analysis.[26] Yao et al. prepared porous polyvinyl alcohol (PVA) dried gel with Au NPs embedded in the network.[27] These gel substrates are 3D ones, showing improved reproducibility and sensitivity. However, the reported preparation methods, such as γ–ray radiation,[25] bacterial synthesis,[26] and dialysis followed by freeze-drying,[28] often need special instrument or are time consuming. It was further noted that little attention was paid to the 3D effective volume in the 3D gel substrates, and their superiority over traditional substrates has not been demonstrated clearly by experimental results, although it was reported the SERS effect was influenced by the gel strength[28] and special environmental changes in such as pH and temperature.[29]

In the present work, we aimed at developing a facile method of fabricating SERS substrates having good sensitivity and homogeneity, and then making use of 3D effective volume rather than nanoscale substrate for SERS detection. Here we proposed a one-pot method for a 3D plasmonic hydrogel substrate without other reducing or crosslinking agent. As a free-standing 3D Ag NPs architecture, the polyvinyl alcohol (PVA) hydrogel encapsulating uniformly-distributed Ag NPs provided a transparent plasmonic network which gave an easy paradigm to realize 3D SERS effective volume. By slice observation as well as depth scanning. For the first time, we monitored a macro scare effective depth in the range to more than one hundred micrometres in the 3D network. Such a great depth may come from harvesting plasmonic effects between active Ag particles couplings in all x, y and z directions. This 3D substrate also demonstrated a good homogeneity in both xy and xz planes, making the hydrogel more reliable and versatile for practical sensing applications. Due to the macro scale effective depth, the substrate exhibited an outstanding ability of tolerating out-of-confocal plane detection and the self-standing bulk structure was very helpful to the real application with portable Raman instruments.

Experimental

Synthetic procedures

The synthesis of the PVA-Ag plasmonic hydrogel substrate began by dissolving PVA powders in distilled water at 90 °C with stirring, followed by quickly adding a specified amount of 0.1 M $AgNO_3$ solution. After incubating for 1 h under stirring, the sol changed in color from colorless to brown. The sol was then transferred to a 96-well plate for shaping. After cooling to room temperature, the PVA-Ag gel was put into a refrigerator to freeze at -18 °C for 2 h. After being thawed at room temperature, the PVA-Ag gel was ready for its use as a SERS substrate. Typically, the mass concentration of PVA in the sol was 15% (wt.), and the concentration of $AgNO_3$ (n, mM) in the PVA sol was varied between 0 and 5 mM. According to the value of n, the obtained PVA-Ag hydrogel was referred to as PVA-nAg hydrogel. For example, PVA-1Ag was obtained when n = 1 mM.

Citrate-Ag sol was prepared using sodium citrate as the reducing agent in accordance with established procedures.[30] Silver nitrate (19 mg) was dissolved in deionised water (100 mL) and heated to boiling. Then sodium citrate (2 mL of a 1% solution) was added dropwise, and heating was maintained for a further 30 min; afterwards, the colloid was cooled to room temperature.

Characterization techniques

The morphology and surface chemical compositions of PVA-Ag were examined with electron microscope (HRTEM, FEI Tecnai G2 20 U-Twin, USA; FE-SEM, HITACHI SU8000, Japan) and an energy-dispersive spectroscopy (EDS, EDAX-FALCON60, USA).

The section cutting of the gel to obtain slices with special thicknesses was performed on a Leica CM3050 S cryostat (Leica, Germany). The temperature was set at -24°C.

SERS measurement

All conventional Raman spectra were measured with a DXR confocal Raman Microscopy equipped with a CCD detector (Thermo Fisher Scientific, USA). The 532 nm and 780 nm line of laser was used as an excitation source. For the 532nm laser, the power was 3.0 mW and the exposure time for each SERS measurement was set at 3 s with 5 accumulations in this study; For the 780 nm laser, the power was 10.0 mW and the exposure time for each SERS measurement was set at 3 s with 10 accumulations, respectively.

Raman mappings and depth-scanning were conducted on a DXRxi Raman Microscopy (Thermo Fisher Scientific, USA). The 532 nm line of laser was used as an excitation source. The laser power was 5.0 mW and the exposure time was set at 3 ms.

The detection of environmental molecules was performed on an Ezrman-M potable Raman spectrometer (Enwave Optronics Inc., USA). A 785 nm laser was used as an excitation source. The laser power was 100 mW and the exposure time for each SERS measurement was set at 3 s with 10 accumulations.

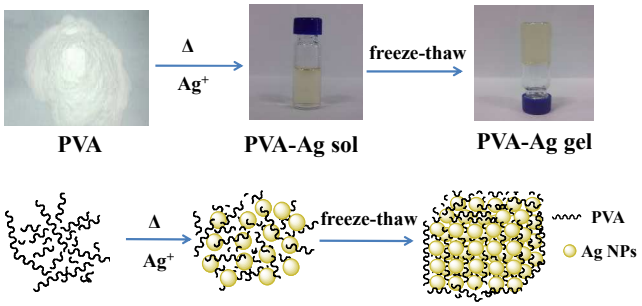

Scheme 1 Preparation procedure of PVA-Ag hydrogel 3D substrate by an *in situ* reduction strategy.

Results and discussion

The preparation process of the PVA-Ag hydrogel was depicted in Scheme 1. PVA is a polymer that can dissolve in water by heating and stirring. A freeze-thaw operation may induce the formation of hydrogen bond between the polymer chains, and hence a physical crosslinking hydrogel can be obtained without using other crosslinking agent.[31] In the synthesis, there were two important steps in the preparation: the Ag^+-reduction induced generation of Ag NPs, and the gelation of Ag NPs distributed PVA sol. The final product

was named PVA-cAg, where c was the used concentration of $AgNO_3$ in unit of mM. By monitoring the UV-visible absorption spectra of the sol, it was found that as the reduction time was prolonged, a strong symmetric absorption peak occurred at about 418 nm and increased in intensity (Fig. 1a), attributed to the SPR peak with Cs symmetry of sphere Ag particles.[32] In addition, the maximum absorption wavelength of the Ag NPs in the sols was red shifted from 418 to 460 nm when the used concentration of $AgNO_3$ was increased from 1 to 5 mM, respectively (Fig. 1b). The red shift of the SPR peak represented an increase of the particle sizes of Ag NPs encapsulated in the hydrogel.[33]

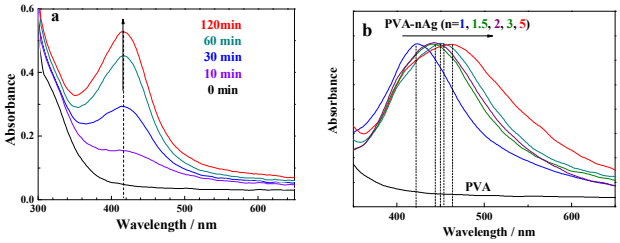

Fig. 1 (a) UV-vis absorption spectra of PVA-1Ag sols in the Ag NPs formation process. The appearing and growing of the absorption peak at 415 nm indicated that more and more Ag NPs were generated in the sols as the reaction time was prolonged. (b) UV-vis absorption spectra of PVA-xAg sols after a reaction for 60 min. Here, the mass concentration of PVA was decreased to 10% in order to easily obtain its UV-vis absorption spectra without gelation. However, the mass concentration of PVA was 15% if not specified elsewhere.

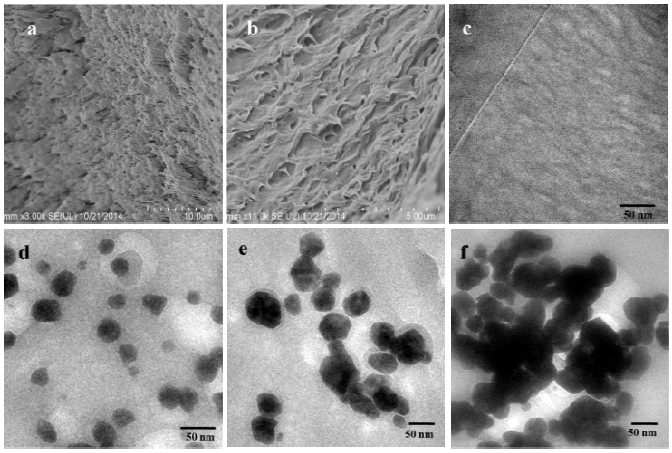

Fig. 2 SEM images of (a) PVA and (b) PVA-2Ag gels, and TEM images of (c) PVA, (d) PVA-1Ag, (e) PVA-2Ag, and (f) PVA-5Ag gels.

After the PVA and PVA-2Ag gels were frooze dried, their micromorphologies were observed by SEM as shown in Figs. 2a and 2b. It was easily found that the plasmonic hydrogel had a porous structure, which will contribute to the easy access and good absorptivity for probe molecules as discussed below. TEM images of the hydrogel slices were also obtained for confirming the distribution of the nano-scale particles. As shown in Figs. 2c-2f, the several tens nanometre particles were well-dispersed in the gels. The EDX spectra confirmed that these particles were Ag NPs (Fig. S1). The sizes of Ag NPs in the gels ranged from 30 to 100 nm, and there was a tendency that more and/or larger Ag NPs were formed when the used concentration of $AgNO_3$ for the preparation was higher which was in accord with the result observed by UV-vis spectra in Fig. 1b.

To evaluate the adsorption properties of PVA-Ag gels, crystal violet (CV) was used as a probe. For the measurement, a piece of weighted PVA-1Ag (150 mg) was immersed in 3.0 mL of 2.5 μM CV solution. After the adsorption for a certain time period, the gel was taken out and rinsed with water, and then subsequently subjected to Raman analysis and the rest solution was used for UV-vis detection. By monitoring the SERS intensity of CV (at 1619 cm^{-1}) on the gel, it was observed that the Raman intensity was initially increased rapidly with prolonging the adsorption time and then saturated beyond about 10 min (curve 1 in Fig. 3). This indicated that the adsorption of CV on the Ag NPs in the PVA-Ag gel substrate was very fast and the adsorption was saturated at 10 min, which was confirmed also by the monitoring of the residual probe concentration through the UV-visible spectrophotometry (curve 2 in Fig. 3). The good absorptivity was also come from the excellent water absorption and swelling ability of PVA hydrogel and the porous structure by the frezee-thaw synthesis procedure.[31] The fast (and strong) adsorption is a great merit of the substrate when it is used as a passive sampling sensor in practical analysis.

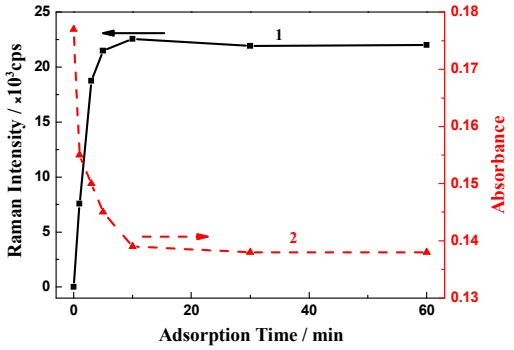

Fig. 3 Time dependences of (1) the SERS intensity (at 1619 cm^{-1}) of PVA-1Ag treated with 2.5 μM CV, and (2) the absorbance of the residual solution at 591 nm (the maximum absorption wavelength of CV).

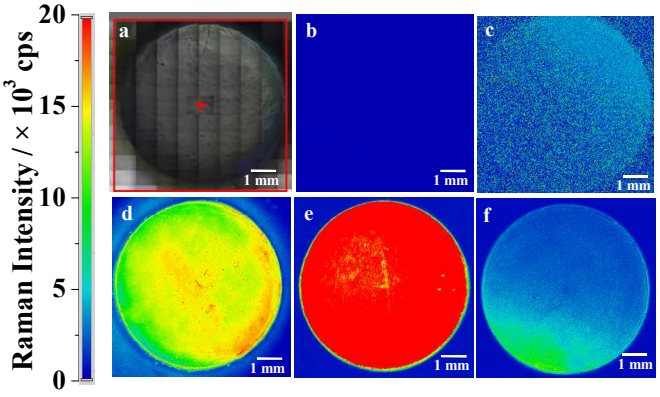

Fig. 4 Raman mapping images of 2.5 μM CV-captured PVA-Ag using the intensity of the 1620 cm^{-1} band. The point-to-point mapping distance in the x and y direction was 10 and 10 μm. (a) white light image of the sample area; (b) PVA-0Ag; (c) PVA-0.5Ag; (d) PVA-1Ag; (e) PVA-2Ag; (f) PVA-5Ag.

Raman mappings were carried out to study the homogeneity and spatial distribution of Ag NPs over the total across area of the gel substrate with CV as the probe. Fig. 4 highlighted the Raman

intensity at 1620 cm^{-1} for different PVA-Ag gels. The mapping was carried out in the area of 8×8 mm^2 with a total of 6.4×10^5 measurement points (i.e., 10×10 μm^2 resolution per measurement point) to obtain a reliable statistic. The Raman maps demnonstrated that the 3D substrates were SERS active across the entire substrate area, and the scattering extent of the intensity values was quite small across the entire subatrate, showing excellent homogeneity.

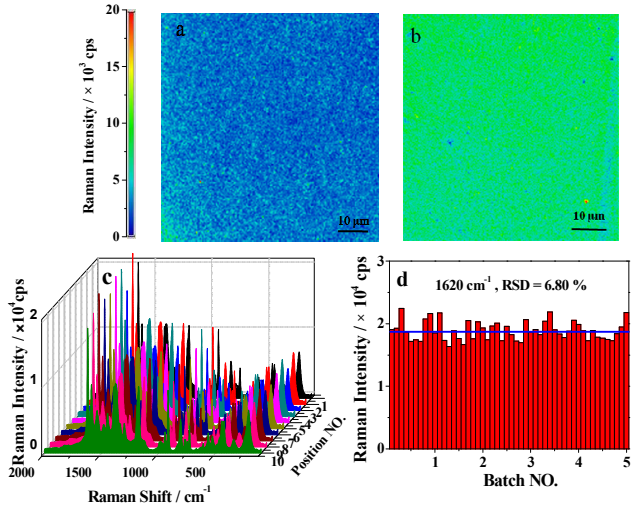

Fig. 5 Homogeneity and reproducibility of PVA-1Ag substrate. (a, b)Distribution map of SERS intensity (at 1620 cm-1) of 2.5 μM CV over PVA-1Ag slices with a thickness of (a) 100 and (b) 200μm. The point-to-point mapping distances in the x and y direction were both 2 μm. (c) SERS spectra of CV (2.5 μM) on PVA-1Ag recorded at 10 spots randomly chosen (see the spot number). (d) SERS intensity (at the 1620 cm^{-1} peak) of 2.5 μM CV on different PVA-1Ag substrates.The different PVA-1Ag substrates were prepared in 5 batches, and the spectrum recording was conducted at 10 spots randomly chosen for each batch substrate. The blue line signed the average intensity of the 10×5 measurements, with a RSD of 6.8%.

For the homogeneity in the internal part, we conducted mappings on the slices obtained from internal part of the substrate, which also confirmed the excellent homogeneity (Figs. 5a, 5b). By prepararing 5 batches of the gel, the point-to-point mapping was further carried out at 10 spots being randomly chosen on the the gel (Figs. 5c, 5d). The 10×5 measurements (5 substrates, and 10 spots on each substrate) produced a relative standard deviation (RSD) of 6.8%. These results indicated that the preparation of the PVA-Ag gel substrate for different batches was quite reproducible, and each substrate sample had good homogeneity for the detection spots. These ensured the reliability of the SERS signal and the practicability of the substrate for real applications. The good homogeneity and reproducibility of our hydrogel substrates may be attributed to the uniform distribution of Ag NPs in the 3D space and the prevention of Ag NP aggregation by the polymer network. In contrast, in the case of Ag NP sol substrates, the uncontrollable aggregation and the coffee-ring effect during the SERS detection caused a very poor reproducibility with RSD values of 30-50% as discussed below.

In order to interrogate the effective depth of the 3D substrate, we performed depth scanning in the x-z plane. The depth from the surface plane to the depth exihibiting highest SERS intensity was defined as the effective depth (H), which represented the depth of the 3D space that effectively contributed to the SERS signal collected at confocal plane. It was exciting that H expanded to several hundred micrometers although traditional 3D substrates reach only to several hundreds of nanometers. Fig. 6 clearly showed the distribution of Raman intensity aross the x-z plane using CV (2.5 μM) as the probe. At a same z position, the intenstiy was indiffernce to the x position, being well consistent with the good homogeneity shown in Fig. 4. At a same x position, however, the intensity was increased initially, passing a maximum, and decreased then with increasing the z depth. This clearly showed the contribution from 3D space. The H values were estimated as 80, 120, 170, 110 and 70 μm for PVA-1Ag, PVA-1.5Ag, PVA-2Ag, PVA-3Ag and PVA-5Ag, respectively. Similar results were obtained when 4-aminothiolphenol (4-ATP, 8 μM) was used instead of CV (Fig. S2). The great H values also proved that the collected SERS signals were not limited on the confocal plane. In fact, the SERS singals near confocal plane might come to confocal plane by scattering of Ag NPs and also are collective.[18]

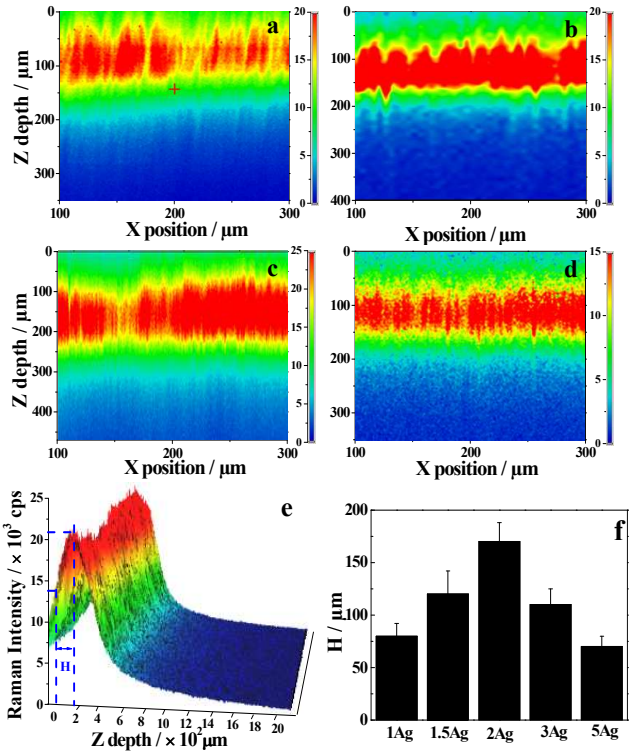

Fig. 6 Raman depth-scanning images of CV-captured PVA-Ag using the 1620 cm^{-1} intensity of CV (2.5 μM). The point-to-point scanning distance in the x and z directions was 5 and 5 μm. (a) PVA-1Ag; (b) PVA-1.5Ag; (c) PVA-2Ag; (d) PVA-3Ag. The colour scale bars gave the Raman peak intensity in unit of 10^3 cps. (e) Typical 3D images of the depth scanning with SERS intensity of PVA-2Ag. (f) Effective depths of different PVA-Ag substrates.

As mentioned above, the effective depths of the substrates were different when different concentrations of Ag salt were used in the substrate preparation. This was because the different Ag salt concentrations led to different in particle sizes and particle densities (as shown in Figs. 1 and 2). It was reported that larger sizes of Ag NPs (<100 nm) are favorable to electromagnetic enhancement[34]. It is certain that higher particle density is favorable to the formation of more hot spots. However, a combination of large particle sizes and a high particle density may decrease of the light transmittance, which

will cause a decrease in the effective depth of the substrate. This makes the 3D substrate be more like a 2D substrate to an extent. Consequently, the Ag salt concentration was optimal at 1~2 mM, but a higher concentration at 5 mM yielded poorer SERS responses.

The macro scale effective space in our 3D network was further confirmed with a "top-down" strategy. Since the hydrogel substrate was a flexible free-standing material, a series of slices with different thicknesses were obtained by employing a section cutting technique, which commonly used in bio-tissue section. The slices were pasted to microscope slide and then immersed in the CV solution (2.5 μM) for 30 min. After rinsed with water, the slices were subjected to Raman analysis. Fig. 7 showed the effects of substrate slice thickness on the SERS intensity (1620 cm^{-1} peak) of PVA-Ag captured with 2.5 μM CV. For both PVA-1Ag and PVA-2Ag, the Raman intensity was linearly increased with increasing the slice thickness from 10 to 350 μm, and tended to be saturated beyond 400μm. The SERS intensity dependence on thickness was another proof for the 3D volume effect. The good linear relation between the SERS intensity and the thickness was also a proof for the homogeneity of the substrate. For the thickness being thinner than the effective depth, the SERS intensity was lower than the saturated intensity since there were not enough Ag NPs that contributed to the SERS signal. When the substrate was thick enough, the deeper space out of the effective volume would not contribute to the signal, leading to a saturation of the SERS intensity for the thickness beyond 400 μm.

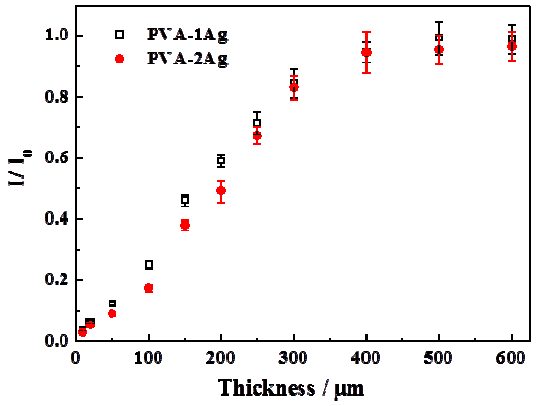

Fig. 7. Effects of hydrogel substrate slice thickness on the SERS intensity at 1620 cm^{-1} of PVA-Ag captured with 2.5 μM CV. The Raman intensity (I) for each slice was normalized with the intensity for the bulk substrate with a thickness of about 1 cm (I_0)

Both the depth scanning and slice observation experiments confirmed the macro scale effective depth in the proposed substrate, but the exact numerical values from the two experiments were different: ~170 μm (Fig. 6) versus 350 μm (Fig. 7). This difference was come from the different signal acquisition modes (Fig. S3). For depth scanning, the laser confocal plane was first at the surface, and then permeated into the hydrogel when the scanning depth (h) was increased. In the transparent architecture, both a circular truncated cone above the confocal plane and a circular truncated cone below the confocal plane contribute to the total SERS intensity collected at the confocal plane (Fig. S3a). However, for the slice observation, the confocal plane was always set at the out surface of the substrate, only a circular truncated cone below the confocal plane contribute to the total SERS intensity (Fig. S3b). If we neglect the influences of the refractive index and light attenuation in the substrate, the upper and lower circular truncated cone should be the same in the volume when the maximum SERS intensity is obtained by the depth scanning mode. This suggests that the effective depth obtained from the depth scanning is about half of that obtained from the slice observation experiment, being well consistent with the experimental results.

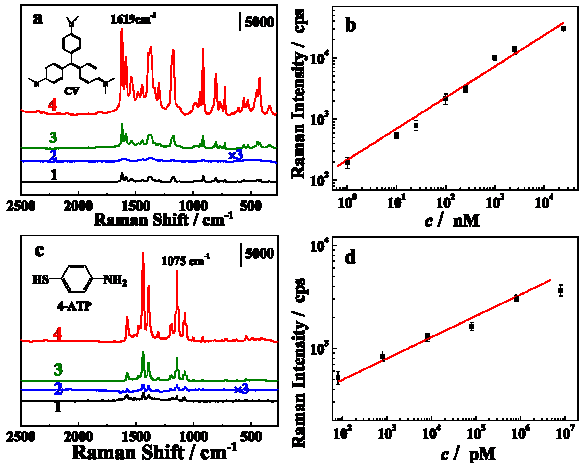

Fig. 8. (a) SERS spectra of CV captured substrates. CV (1) 2.5×10^{-6} M on citrate-Ag sol; (2) 1.0×10^{-9} M, (3) 2.5×10^{-7} and (4) 2.5×10^{-6} M on PVA-2Ag hydrogel substrates. (b) Effects of CV concentration on its Raman peak intensity (at 1619 cm^{-1}) on PVA-2Ag hydrogel substrate. (c) SERS spectra of 4-ATP captured substrates. 4-ATP (1) 8.0×10^{-6} M on citrate-Ag sol; (2) 8.0×10^{-13}, (3) 8.0×10^{-9} and (4) 8.0×10^{-6} M on PVA-2Ag hydrogel substrates. (d) Effects of 4-ATP concentration on its Raman peak intensity (at 1075 cm^{-1}) on PVA-2Ag hydrogel substrate.

To evaluate the sensitivity of the hydrogel 3D substrate, the Raman responses of two probes CV and 4-ATP were acquired on a DXR confocal Raman Microscope (Thermo Fisher Scientific, USA). For comparison, we also obtained the SERS spetrum with common used citrate-Ag sol substrate at the same condition.[30] The SERS spectrum of CV (2.5 μM) on the citrate-Ag and PVA-2Ag substrates were shown in Fig. 8a (spectra 1 and 3). A much better enhancemnt was obtained on PVA-2Ag. Similar detection of 8.0 μM 4-ATP instead of CV also confirmed this (Fig. 8c). By analyzing the SERS spectra of PVA-1Ag captured with CV or 4-ATP at different concentrations, it was found that the spectral feature characteristics of CV and 4-ATP were clearly observable at a trace concentration of 1 nM and 0.8 pM, respectively. The observed detection limit was much lower than that reported on literature (500 nM and 0.5 nM).[35] Moreover, there were good linear corelations between the logarithm of Raman peak intensity of CV (at 1619 cm^{-1}) and the logarithm of CV concentration in the range of $1–1\times10^4$ nM, and between the logarithm of Raman peak intensity of 4-ATP (at 1075 cm^{-1}) and the logarithm of 4-ATP concentration in the range of 10^2 to 1×10^6 pM. These results demonstrate that the new macro-scale 3D substrate provide excelllent SERS performances in the quantitative analysis of organic small molecules with ultra-sensitivity.

Such a high sensitivity may be attributed to the volume effect of the macro-3D structure. It is known that the greatest absolute field enhancement at asperities such as apexes of triangles or the corners of cubes or at the nanoscale gap (<10 nm) between dimers is most important for single molecule detection. A recent study showed that

stronger SERS response was observed from large (10-30 nm) gap distance difined by large (>150 nm) structures wihch came from a great number of molecule contained in the large hot spot with great averge field enhancement.[15] In our case, Ag NPs were uniformly distributed in the hydrogel network, the coupling of their electronic fields would occur in all x, y, and z directions, resulting in great average field over the whole substrate region within the effective volume, which, together with good light transmittance, provided a great SERS enhancement.

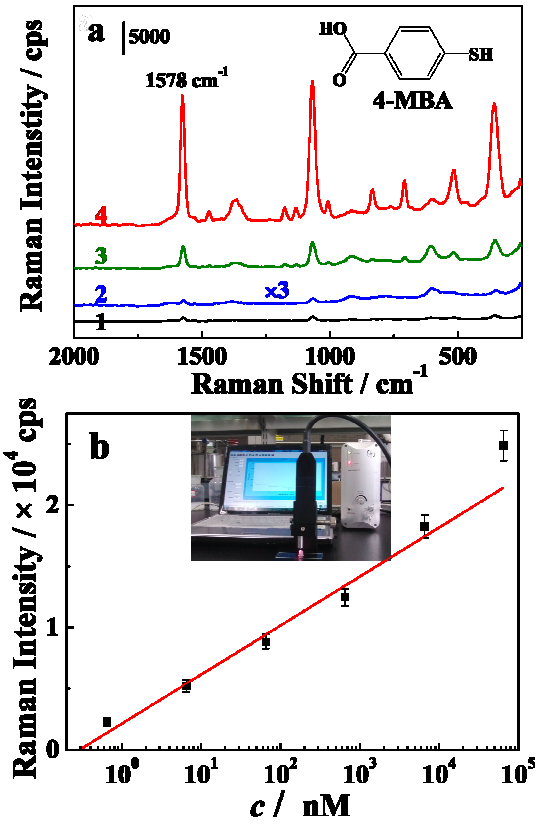

Fig. 9 Detection of 4-MBA using a portable Raman instrument. (a) SERS spectra of 4-MBA captured substrates: (1) 2.5 $\times 10^{-6}$ M 4-MBA on citrate-Ag sol; (2) 6.5×10^{-11}, (3) 6.5×10^{-7} and (4) 6.5×10^{-5} M 4-MBA on PVA-2Ag hydrogel substrate. b) The concentration dependence of the SERS intensity at 1578 cm^{-1}. Inset: the used portable Raman instrument.

The prominent characteristics of the novel 3D substrate will be strenghened when it is used for practical on-site applications on portable Raman spectrometers without a confocal system, because more signal would be effectively collected in the transparent hydrogel by an optic fiber probe. The spectra of 4-ATP were obtained on the 3D hydrogel substrate in comparison with a commonly used citrate-Ag NPs sol substrate[30] on the two different instruments. On either the confocal or non-confocal Raman instrument, the 3D substrate yielded much stronger SERS responses than the citrate-Ag sol substrate did by a magnitude of about 2 orders (Fig. S4). Moreover, when the measurements were conducted at 20 randomly-selected spots, the RSD was only about 7% on the hydrogel substrate, whereas the RSD was increased to about 50% on the citrate-Ag sol substrate. During the measuring process, the gradual evaporation of water led to uncontrollable changes in intensity for the citrate-Ag sol substrate. Therefore, the hydrogel 3D substrate is a better candidate for both qualitative and quantitative detections of analytes.

The on-site detection of environmental pollutants 4-mercapto-benzoic acid (4-MBA) and 2,2-dipyridyl was conducted on the portable Raman spectrometer using PVA-2Ag as the substrate. As shown in Fig. 9 (and Fig. S5), the substrate showed excellent performance for the detection, yielding a limit of detection of 65 pM and 6.4 nM for 4-MBA and 2,2-dipyridyl, respectively. A linear relation between the intensity at 1578 cm^{-1} of 4-MBA and the logarithm of the concentrations over the range of $10–10^4$ nM was obtained. The selfstanding substrate is very conveninent to be separated from the detection solution, which is preferable for on-site detection, due to its shortened detection time. Therefore, this provides a valuable tool for fast monitoring.

Conclusions

In summarization, we demonstrated a green facile route for fabricating a novel macro-scale 3D hydrogel substrate which required a minimal fabrication effort and offered fully accessibility for practical SERS substrate synthesis. With help of the PVA network, the in situ generated Ag NPs were uniformly dispersed in the entire substrate, which ensured the excellent homogeneity and reproducibility. In particular, a macro scale effective depth was confirmed by depth scanning and slice observation, which may come from the compensate effect by Ag NPs uniformly dispersed in the laser path, the coupling of their electronic fields would occur in all x, y, and z directions, resulting in great average field in the whole substrate region. Such a huge effective depth made the substrate outstanding among the traditional low dimensional as well as nanoscale 3D structures, with highly sensitivity and enhanced tolerable ability toward out-of-focus laser position at the sample. The self-standing substrate has been successfully applied in detection of trace pollutants with both confocal and portable Raman instruments, exhibiting its potential as an effective substrate for cheap, rapid, sensitive, and reliable SERS detection and sensing. The insight into the macro-scale effective space gives a promising direction for design of 3D SERS substrate for practical applications.

Acknowledgements

This work was supported by the National High Technology Research and Development Program of China (863 Program) (Grant No. 2012AA06A304) and the National Science Foundation of China (Grant Nos. 21177044 and 21377169).

Notes and references

[a] School of Chemistry and Chemical Engineering, Huazhong University of Science and Technology, Wuhan 430074 (P. R. China)
[b] Key Laboratory of Catalysis and Materials Science of the State Ethnic Affairs Commission and Ministry of Education, College of Chemistry and Materials Science, South Central University for Nationalities, Wuhan 430074 (P. R. China)
[c] Department of Chemistry, University of Duisburg-Essen, 45141 Essen (Germany)

* Corresponding authors: E-mail: lhzhu63@hust.edu.cn (L. Zhu); E-mail: tangheqing@mail.scuec.edu.cn (H. Tang)

Electronic Supplementary Information (ESI) available: difference between "active depth" and "effective depth", EDX spectrum, depth scanning for 4-ATP, Illustration of different detect modes, Analyte detection. See DOI: 10.1039 /c000000x/

1 (a) E. C. Lin, J. Fang, S. C. Park, T. Stauden, J. Pezoldt and H. O. Jacobs, *Adv. Mater.*, 2013, **25**, 3554;(b) M. Li, S. K. Cushing, J. Zhang, S. Suri, R. Evans, W. P. Petros, L. F. Gibson, D. Ma, Y. Liu and N. Wu, *ACS Nano,* 2013, **7**, 4967; (c) Y. W. Zhang, S. Liu, L. Wang, X. Y. Qin, J. Q. Tian, W. Lu, G. H. Chang and X. P. Sun, *RSC Adv.*, 2012, **2**, 538.

2 (a) Y. Zhang, Y. Huang, F. Zhai, R. Du, Y. Liu and K. Lai, *Food Chem.*, 2012, **135**, 845; (b) L. He, E. Lamont, B. Veeregowda, S. Sreevatsan, C. L. Haynes, F. Diez-Gonzalez and T. P. Labuza, *Chem. Sci.*, 2011, **2**, 1579.

3 (a) E.-C. Lin, J. Fang, S.-C. Park, F. W. Johnson and H. O. Jacobs, *Nat. Commun.,* 2013, **4**, 1636; (b) R. Alvarez-Puebla and L. Liz-Marzan, *Energy Environ. Sci.*, 2010, **3**, 1011;

4 (a) R. W. Taylor, R. J. Coulston, F. Biedermann, S. Mahajan, J. J. Baumberg, and O. A. Scherman, *Nano Lett.,* 2013, **13**, 5985; (b) W. Xie, C. Herrmann, K. Kömpe, M. Haase and S. Schlücker, *J. Am. Chem. Soc.*, 2011, **133**, 19302.

5 (a) S. Zong, Z. Wang, H. Chen, J. Yang and Y. Cui, *Anal. Chem.,* 2013, **85**, 2223; (b) X. Qian, X.-H. Peng, D. O. Ansari, Q. Yin-Goen, G. Z. Chen, D. M. Shin, L. Yang, A. N. Young, M. D. Wang and S. Nie, *Nat. Biotechnol.*, 2008, **26**, 83.

6 (a) K. V. Kong, Z. Lam, W. K. O. Lau, W. K. Leong and M. Olivo, *J. Am. Chem. Soc.,* 2013, **135**, 18028; (b) W. Ma, H. Yin, L. Xu, X. Wu, H. Kuang, L. Wang and C. Xu, *Chem. Common.*, 2014, **50**, 9737.

7 (a) X. Wang, M. Li, L. Meng, K. Lin, J. Feng, T. Huang, Z. Yang and B. Ren, *ACS Nano,* 2014, **8**, 528; (b) Rongchao Jin, *Angew. Chem. Int. Ed.,* 2010, **49**, 2826.

8 (a) J. Ye, F. Wen, H. Sobhani, J. B. Lassiter, P. V. Dorpe, P. Nordlander and N. J. Halas, *Nano Lett.,* 2012, **12**, 1660; (b) Y. Yao, Y. Zhou, J. Dai, S. Yue and M. Xue, *Chem. Commun.*, 2014, **50**, 869.

9 (a) M. P. Cecchini, V. A. Turek, J. Paget, A. A. Kornyshev and J. B. Edel, *Nat. Mater.,* 2012, **12**, 165; (b) L. Su, W. Z. Jia, D. P. Manuzzi, L. C. Zhang, X. P. Li, Z. Y. Gu and Y. Lei, *RSC Adv.*, 2012, **2**, 1439.

10 (a) T. K. Sau, A. L. Rogach, F. Jäckel, T. A. Klar and J. Feldmann, *Adv. Mater.,* 2010, **22**, 1805; (b) H. Wang, C. S. Levin and N. J. Halas, *J. Am. Chem. Soc.,* 2005, **127**, 14992.

11 B. Wiley, Y. Sun, B. Mayers and Y. Xia, *Chem.- Eur. J.,* 2005, **11**, 454.

12 V. T. Cong, E.O. Ganbold, J. K. Saha, J. Jang, J. Min, J. Choo, S. Kim, Nam W. Song, S. J. Son, S. B. Lee and S. W. Joo, *J. Am. Chem. Soc.*, 2014, **136**, 3833.

13 L. Polavarapu and L. M. Liz-Marzan, *Phys. Chem. Chem. Phys.,* 2013, **15**, 5288.

14 (a) L. Ouyang, L. Zhu, J. Jiang and H. Tang, *Anal. Chim. Acta,* 2014, **816**, 41; (b) J. Jiang, L. Ouyang, L. Zhu, J. Zhou and H. Tang, *Sci. Rep.,* 2014, **4**, 3942.

15 K. A. Atoerzinger, J. Y. Lin and T. W. Odom, *Chem. Sci.*, 2011, **2**, 1435.

16 H. Xu, J. Aizpurua, M. Kall and P. Apell, *Phys. Rev. E: Stat. Phys., Plasmas, Fluids, Relat. Interdiscip. Top.*, 2000, **62**, 4318.

17 (a) H. Tang, G. Meng, Q. Huang, Z. Zhang, Z. Huang and C. Zhu, *Adv. Funct.Mater.,* 2012, **22**, 218; (b) R. Li, C. Han and Q. W. Chen, *RSC Adv.*, 2013, **3**, 11715; (c) A. Yang, J. L. Bi, S. C. Yang, J. Zhang, A. R. Chen and S. H. Liang, *RSC Adv.*, 2014, **4**, 45856.

18 S. Lee, M. G. Hahm, R. Vajtai, D. P. Hashim, T. Thurakitseree, A. C. Chipara, P. M. Ajayan and J. H. Hafner, *Adv. Mater.*, 2012, **24**, 5261.

19 F. Shao, Z. Lu, C. Liu, H. Han, K. Chen, W. Li, Q. He, H. Peng and J. Chen, *ACS Appl. Mater Interfaces,* 2014. **6**, 6281.

20 M. Chen, I. Y. Phang, M. R. Lee, J. K. W. Yang and X. Y. Ling, *Langmuir,* 2013, **29**, 7061.

21 M. Chirumamilla, A. Toma, A. Gopalakrishnan, G. Das, R. P. Zaccaria, R. Krahne, E. Rondanina, M. Leoncini, C. Liberale and F. De Angelis, *Adv. Mater.,* 2014, **26**, 2353.

22 (a) V. Ntziachristos, *Nat. Methods,* 2010, **7**, 603; (b) S. Keren, C. Zavaleta, Z. Cheng, A. de la Zerda, O. Gheysens and S. S. Gambhir, *PNAS,* 2008, **105**, 5844.

23 L. Bao, P. Sheng, J. Li, S. Wu, Q. Cai and S. Yao, *Analyst*, 2012, **137**, 4010.

24 A. C. Manikas, G. Romeo, A. Papa and P.A. Netti, *Langmuir*, 2014, **30**, 3869.

25 K. Shin, K. Ryu, H. Lee, K. Kim, H. Chung and D. Sohn, *Analyst*, 2013, **138**, 932.

26 M. Park, H. Chang, D. H. Jeong and J. Hyun, *BioChip J.*, 2013, **7**, 234.

27 S. Yao, C. Zhou and D. Chen, *Chem. Commun.*, 2013, **49**, 6409.

28 S. Fateixa, A. L. Daniel-da-Sila, H. I. S. Nogueira and T. Trindade, *J. Phys. Chem. C,* 2014, **118**, 10384.

29 (a) C. Jiang, Y. Qian, Q. Gao, J. Dong and W. Qian, *J. Mater. Chem.*, 2010, **20**, 8711; (b) X. Y. Liu, C. Zhang, J. M. Yang, D. L. Lin, L. Zhang, X. Chen and L. S. Zha, *RSC Adv.*, 2013, **3**, 3384.

30 P. C. Lee and D. Meise, *J. Phys. Chem.*, 1982, 86, 3391.

31 E. Yokoyama, I. Masada, K. Shimamura, T. Ikawa, and K. Monobe, *Cololid Polym. Sci.,* 1986, **264**, 595.

32 L. Guerrini and D. Graham, *Chem. Soc. Rev*,. 2012, **41**, 7085.

33 M. Rycenga, M. R. Langille, M. L. Personick, T. Ozel and C. A. Mirkin, *Nano Lett.*, 2012, **12**, 6218.

34 Y. Zhou, X. Cheng, D. Du, J. Yang, N. Zhao, S. Ma, T. Zhong and Y. Lin, *J. Mater. Chem. C*, 2014, **2**, 6850.

35 (a) A. Kudelski, *Chem. Phys. Lett.,* 2005,**414**, 271; (b) W. Zhai, D. Li, L Qu, J. S. Fossey and Y. Long, *Nanoscale*, 2012, **4**, 137.